Rare *De Novo* Missense Variants in RNA Helicase DDX6 Cause Intellectual Disability and Dysmorphic Features and Lead to P-Body Defects and RNA Dysregulation

Chris Balak,[1,2,23,*] Marianne Benard,[3,23] Elise Schaefer,[4,11,23] Sumaiya Iqbal,[5,6] Keri Ramsey,[1,2] Michèle Ernoult-Lange,[3] Francesca Mattioli,[7,8,9,10] Lorida Llaci,[1,2] Véronique Geoffroy,[11] Maité Courel,[3] Marcus Naymik,[1,2] Kristine K. Bachman,[12] Rolph Pfundt,[13] Patrick Rump,[14] Johanna ter Beest,[13] Ingrid M. Wentzensen,[15] Kristin G. Monaghan,[15] Kirsty McWalter,[15] Ryan Richholt,[1] Antony Le Béchec,[16] Wayne Jepsen,[1,2] Matt De Both,[1,2] Newell Belnap,[2] Anne Boland,[17] Ignazio S. Piras,[1,2] Jean-François Deleuze,[17] Szabolcs Szelinger,[1,2] Hélène Dollfus,[4,11] Jamel Chelly,[7,8,9,10,18] Jean Muller,[11,18] Arthur Campbell,[5,6] Dennis Lal,[5,6,19,20,21] Sampathkumar Rangasamy,[1,2] Jean-Louis Mandel,[7,8,9,10,22] Vinodh Narayanan,[1,2,24] Matt Huentelman,[1,2,24] Dominique Weil,[3,24] and Amélie Piton[7,8,9,10,19,24,*]

The human RNA helicase *DDX6* is an essential component of membrane-less organelles called processing bodies (PBs). PBs are involved in mRNA metabolic processes including translational repression via coordinated storage of mRNAs. Previous studies in human cell lines have implicated altered DDX6 in molecular and cellular dysfunction, but clinical consequences and pathogenesis in humans have yet to be described. Here, we report the identification of five rare *de novo* missense variants in *DDX6* in probands presenting with intellectual disability, developmental delay, and similar dysmorphic features including telecanthus, epicanthus, arched eyebrows, and low-set ears. All five missense variants (p.His372Arg, p.Arg373Gln, p.Cys390Arg, p.Thr391Ile, and p.Thr391Pro) are located in two conserved motifs of the RecA-2 domain of DDX6 involved in RNA binding, helicase activity, and protein-partner binding. We use functional studies to demonstrate that the first variants identified (p.Arg373Gln and p.Cys390Arg) cause significant defects in PB assembly in primary fibroblast and model human cell lines. These variants' interactions with several protein partners were also disrupted in immunoprecipitation assays. Further investigation via complementation assays included the additional variants p.Thr391Ile and p.Thr391Pro, both of which, similarly to p.Arg373Gln and p.Cys390Arg, demonstrated significant defects in P-body assembly. Complementing these molecular findings, modeling of the variants on solved protein structures showed distinct spatial clustering near known protein binding regions. Collectively, our clinical and molecular data describe a neurodevelopmental syndrome associated with pathogenic missense variants in *DDX6*. Additionally, we suggest *DDX6* join the DExD/H-box genes *DDX3X* and *DHX30* in an emerging class of neurodevelopmental disorders involving RNA helicases.

Introduction

Intellectual disability (ID) is a result of abnormal neurodevelopment and affects at least 1% of the population. ID typically presents in the first few years of life and is characterized by impairments in cognition and adaptive behavior. It is often accompanied by further delays in language and motor skills (developmental delay [DD]), as seen in many neurodevelopmental disorders (NDDs). Given the complexity of central nervous system development, the genetic contribution to ID is quite heterogeneous. Pathogenic variants in several hundred genes are now involved in monogenic forms of ID, and each is responsible for a subset of individuals.[1]

The widespread use of high-throughput sequencing has allowed for a considerable increase in the identification of these pathogenic variants. Large-scale studies that utilize whole-exome sequencing (WES) or whole-genome

[1]Translational Genomics Research Institute, Neurogenomics Division, Phoenix, AZ 85004, USA; [2]Translational Genomics Research Institute's Center for Rare Childhood Disorders, Phoenix, AZ 85012, USA; [3]Sorbonne Université, CNRS, Institut de Biologie Paris-Seine, Laboratoire de Biologie du Développement, F-75005 Paris, France; [4]Medical Genetics Department, University Hospitals of Strasbourg, the Institute of Medical Genetics of Alsace, 67000 Strasbourg, France; [5]Stanley Center for Psychiatric Research, Broad Institute of MIT and Harvard, Cambridge, MA 02142, USA; [6]Analytic and Translational Genetics Unit, Massachusetts General Hospital, Boston, MA 02114, USA; [7]Institute of Genetics and Molecular and Cellular Biology, Illkirch, France; [8]French National Center for Scientific Research, UMR7104, 67400 Illkirch, France; [9]National Institute of Health and Medical Research U964, 67400 Illkirch, France; [10]University of Strasbourg, 67081 Illkirch, France; [11]Laboratoire de Génétique Médicale, Institut de Génétique Médicale d'Alsace, INSERM U1112, Fédération de Médecine Translationnelle de Strasbourg, Université de Strasbourg, 67081 Strasbourg, France; [12]Geisinger Medical Center, Dansville, PA 17822, USA; [13]Department of Genetics, University Medical Center Groningen, University of Groningen, 9713 GZ Groningen, the Netherlands; [14]Radboud University Nijmegen Medical Center, Department of Human Genetics, Division of Genome Diagnostics, 6525 GA Nijmegen, the Netherlands; [15]GeneDx, Gaithersburg, MD 20877, USA; [16]Medical Bioinformatics Unit, UF7363, Strasbourg University Hospital, 67000 Strasbourg, France; [17]Centre National de Recherche en Génomique Humaine, Institut de Biologie François Jacob, CEA, Université Paris-Saclay, F-91057, Evry, France; [18]Molecular Genetics Unit, Strasbourg University Hospital, 67000 Strasbourg, France; [19]Epilepsy Center, Neurological Institute, Cleveland Clinic, Cleveland, OH 44195, USA; [20]Genomic Medicine Institute, Lerner Research Institute Cleveland Clinic, Cleveland, OH 44195, USA; [21]Cologne Center for Genomics, University of Cologne, 50931 Cologne, Germany; [22]University of Strasbourg Institute of Advanced Studies, 67081 Strasbourg, France
[23]These authors contributed equally to this work
[24]These authors contributed equally to this work
*Correspondence: piton@igbmc.fr (A.P.), cbalak@ucsd.edu (C.B.)
https://doi.org/10.1016/j.ajhg.2019.07.010.

sequencing (WGS) to look for pathogenic *de novo* variants involved in autosomal-dominant forms of ID and NDD continue to be performed, but these have focused more on loss-of-function (LoF) variants. Hence, we can expect that most genes sensitive to LoF events will be identified in the next few years. On the contrary, identification of missense variants that lead to ID or NDDs will continue for some time because of the difficulty of defining pathogenicity from large-scale sequencing data. *In silico* analyses such as spatial clustering studies will help to identify novel genes with clustered *de novo* pathogenic missense variants,[2] but there remains a necessity for variant-specific functional studies to confidently demonstrate cellular dysfunction.

The hundreds of genes with pathogenic variants implicated in ID encode proteins involved in different neuron-specific or ubiquitous cellular processes: synaptic function and architecture, cytoskeleton remodeling, regulation of transcription through chromatin remodeling, or mRNA posttranscriptional regulation such as maturation, export, degradation, translation, etc.[1,3,4] In eukaryotic cells, this post-transcriptional regulation of gene expression is essential to proper neurodevelopment. A large variety of RNA-binding proteins (RBPs) control mRNA localization, translation, storage, and decay in the cytoplasm, thus enabling the spatio-temporal adjustment of protein synthesis depending on cellular needs. One of the most illustrative examples of how alterations of mRNA metabolism can lead to NDD is Fragile-X syndrome, caused by pathogenic variants in the gene *FMR1*,[5] a gene encoding the FMRP protein, which is involved in the regulation of mRNA transport and translation.[6]

In this study, we have assembled a cohort of children with ID and other similar features who harbor rare *de novo* variants in a single exon of *DEAD-box helicase 6* (*DDX6,* MIM: 600326), a gene involved in RNA metabolism. The *DDX6* gene encodes an RNA helicase within the Helicase Superfamily 2 (SF2).[7] SF2 helicases function on RNA in an ATP-dependent fashion. The helicases are characterized by the presence of two RecA-like globular domains, ancient protein construction modules found in many motor-type proteins, that transit on or remodel RNA and DNA. The domains are connected by a flexible linker, and together they form a cleft for ATP and RNA binding. Within SF2, the DExD/H-box helicases (DEAD, DEAH, DExH. and DExD) are a subfamily sharing at least eight conserved motifs and slight variations of the signature helicase motif II for which they are named. There are 50 DDX/DHX helicases in humans.[8] Whereas most of them are functionally uncharacterized, the data available so far indicate that they have highly specific functions.

DDX6 in particular is a DEAD-box protein characterized in part by its Asp-Glu-Ala-Asp (DEAD)[7] motif, and it is involved in the regulation of mRNA decay and translation.[9] It is also essential for forming cytosolic membraneless ribonucleoprotein (RNP) granules called processing bodies (P-bodies or PBs),[10,11] which are involved in RNA metabolism through the coordinated storage of mRNAs that encode regulatory functions.[12,13] P-bodies are observed in all eukaryotes. Like other RNP granules, such as stress granules, germ granules, and neuronal granules, their formation relies on RNA-protein networks, multivalent low-affinity interactions, and liquid-liquid phase separation. Nevertheless, each RNP granule is distinct in its composition and function. Currently, no neurological diseases have been associated with P-body defects. We present here the clinical phenotypes of individuals harboring rare *DDX6* missense variants and functional studies that indicate these variants affect DDX6 function in terms of mRNA decay and PB assembly, leading to a neurodevelopmental *DDX6* syndrome.

Subjects and Methods

Subjects

Whole blood, saliva, buccal cells, skin fibroblasts, and/or photos were obtained from research participants subsequent to informed consent. The research on individuals within this study was performed according to research protocols approved by the institutional review boards or local ethics committees of the Translational Genomics Research Institute (TGen) and TGen's Center for Rare Childhood Disorders (C4RCD) (subjects 1 and 4), Strasbourg University Hospital (subject 2), and the Groningen University and Radboud University Nijmegen Medical Centers (subject 5). All research participants and research groups, excluding subject 5, were connected through GeneMatcher.[14]

DNA Sequencing and Bioinformatic Processing

This study involves subjects and data from five unrelated families at different institutions in the US and Europe. Subject 1 and parents underwent WES at TGen. Genomic DNA was extracted from peripheral blood then isolated in a CLIA lab with the DNeasy extraction kit (QIAGEN). Libraries were prepared with the Hyper DNA Prep Kit for Illumina Platforms (Kapa Biosystems). Exome capture was performed with the SureSelectXT Target Enrichment Platform with Clinical Research Exome baits (Agilent Technologies). Sequencing was performed by 100 base pair (bp) paired-end sequencing on a HiSeq4000 instrument (Illumina). Reads were aligned to the human genome (Hg19/GRCh37) with the Burrows-Wheeler Aligner (BWA mem v.0.7.8).[15] PCR duplicates were identified with Picard MarkDuplicates v1.79. Base quality recalibration and indel realignment were performed with the Genome Analysis Toolkit (GATK v3.5-1).[16] Variants were jointly called with HaplotypeCaller and recalibrated with GATK[17]. Quality controls were conducted with FASTQC v0.11.5. Called variants were annotated with SnpEff v3.0a[18] against Ensembl GRCh37.66 and filtered against dbSNP137 1000 Genomes Project (minor allele frequency < 0.05), SnpEff Impact: high + moderate, GATK quality score > 300, and known genes. We used prediction scores from dbNSFP (Database for Nonsynonymous SNP's Functional Predictions) and an internal annotation tool for filtering. Subject 2 underwent a simplex WES (Dijon Hospital) as previously described.[19] When no pathogenic variant was found, trio WGS was performed at the Centre National de Recherche en Génomique Humaine (CNRGH). Libraries were prepared and sequenced

with the Illumina TruSeq DNA PCR-Free Library Preparation Kit and sequenced (3 lanes/genome, paired-end 100 bp) on a HiSeq2000 platform from Illumina (Illumina) to obtain a depth of 30× for each sample. Reads were aligned on the human genome (GRCh37) with bwa software,[15] duplicate sequences were filtered out with Sambamba tools, and an additional step of realignment was performed with GATK programs (IndelRealigner). Variants were identified via 4 programs (UnifiedGenotyper and HaplotypeCaller from GATK, Platypus,[20] and Samtools). Single nucleotide variations (SNVs) falling in a coding region or in a genomic region of a known ID gene were annotated with Varank;[21] annotations included information about the inheritance (*de novo* versus inherited variants). Comparison of SNVs identified genome-wide in the proband and his parents resulted in a list of potential *de novo* variants. Structural variants were detected with SoftSV[22] and copy number variants with CANOES,[23] and then variants were annotated by AnnotSV.[24] For subject 4, genomic DNA from the proband and respective parents was sequenced at GeneDx. The exonic regions and flanking splice junctions of the genome were captured with the IDT xGen Exome Research Panel v1.0. Massively parallel (NextGen) sequencing was done on an Illumina system with 100 bp or greater paired-end reads. Reads were aligned to human genome build GRCh37/hg19 and analyzed for sequence variants with a custom-developed analysis tool. Additional sequencing technology and variant interpretation protocol has been previously described.[25] The general assertion criteria for variant classification are publicly available on the GeneDx ClinVar submission page (see Web Resources). Subject 5 and parents underwent trio WES. We used Sanger sequencing to confirm *DDX6* variants in all affected probands.

Variant Prioritization and Analysis

Candidate variants were categorized into inheritance patterns, including *de novo*, recessive, compound heterozygous, and X-linked, and prioritized by various methods including variant frequency (less than 2% or absent) via the Genome Aggregation Database (gnomAD).[26] We performed further filtering of candidate genes and variants from the prediction of damaging effects by using *in silico* tools such as the gnomAD v2.1.1 probability of loss-of-function intolerance score (O/E, pLI) and missense *Z* score, Combined Annotation Dependent Depletion (CADD),[27] Genomic Evolutionary Rate Profiling (GERP),[28] SIFT,[29] PolyPhen 2,[30] SNAP2,[31] Envision,[32] biological relevance, and association with human disorders with a neurodevelopmental phenotype in the literature. Candidate variants were interpreted according to the guidelines published by the American College of Medical Genetics and Genomics (ACMG).[33]

RNA Sequencing and Gene Expression Analysis of Fibroblasts

Experiments were performed in duplicate from two different fibroblast pellets obtained from subject 2 (S2). Total RNA was extracted with the RNeasy mini kit (QIAGEN), including a DNase treatment. RNA levels and quality were quantified with a Nanodrop spectrophotometer and a 2100 Bioanalyzer (Agilent). mRNA libraries of template molecules suitable for high-throughput DNA sequencing were created with the TruSeq RNA Sample Preparation v2 Kit from 200 ng of total RNA. S2 was prepped with eight other individuals affected by Bardet Biedl syndrome or other causes of ID not related to *DDX6* mutation, and the subsequent libraries were sequenced on one run with the Illumina Hiseq 4000 sequencer as paired-end 100 base reads. Image analysis and base calling were performed with RTA 1.18.61 and CASAVA 1.8.2. Reads (403,718,870 and 299,879,030) were mapped onto the hg19 assembly of the human genome with TopHat 2.0.14 and the Bowtie 2-2.1.0 aligner. The raw sequencing data generated in the course of this RNA study are not publicly available, but more details are available on demand. Gene expression was quantified with HTSeq-0.6.1[34] and gene annotations from Ensembl release 75. Only uniquely-mapped and non-ambiguously assigned reads were retained for further analyses. Read counts were then normalized across libraries with the median-of-ratios method proposed by Anders and Huber.[35] To check whether the normalization was correctly performed, relative log expression (RLE) plots were drawn to check that the distributions are centered around the zero line and as tight as possible. Comparisons to the eight aforementioned individuals with other neurodevelopmental or sensorineural conditions unrelated to *DDX6* mutation were performed according to the statistical method proposed by Anders and Huber.[35] We used the Wald test to estimate the p values, and we adjusted them for multiple testing with the Benjamini and Hochberg method.[36] Significant differentially-expressed (DE) genes were analyzed with the Database for Annotation, Visualization, and Integrated Discovery (DAVID 6.7). We used biological processes and molecular functions of the Gene Ontology Consortium (GO), as well as pathways from KEGG (Kyoto Encyclopedia of Genes and Genomes), for the functional annotations. The list of genes known or suspected to be involved in ID was extracted from the SysID database (see Web Resources). Genes with ten or more reads detected (on average) were considered as expressed in fibroblasts.

Molecular Modeling of *DDX6* and Missense Variant Impact Prediction

High-resolution crystal structures for human DDX6 in an open conformation (PDB: 4CT5) and closed conformation in complex with the CNOT1 MIF4G and 4E-T CHD domains (PDB: 5ANR) were obtained from Protein Data Bank (originally submitted by Mathys et al.[37] and Ozgur et al.[9]). Three-dimensional (3D) mapping of gnomAD v2.1.1 missense variants and DDX6 variants c.1115A>G (p.His372Arg), c.1118G>A (p.Arg373Gln), c.1168T>C (p.Cys390Arg), c.1171A>C (p.Thr391Pro), and c.1172C>T (p.Thr391Ile) was performed with PyMOL v2.1.1 and the UCSF Chimera package.[38]

Cell Culture, siRNA, Plasmids, and Transfection

Fibroblasts from Subject 2 and one sex-matched control individual, as well as fibroblasts from subject 1 and her parents, were maintained in 50% low-glucose DMEM and 50% nutrient mixture F10-Ham, supplemented with 10% fetal calf serum and 1% penicillin and streptomycin. Human embryonic kidney HEK293 and human epithelioid carcinoma HeLa cells were maintained in high-glucose DMEM supplemented with 10% fetal calf serum and 1% penicillin and streptomycin.

To silence endogenous *DDX6*, HeLa cells were transfected via Lullaby (OZ Biosciences) at the time of their plating with 0.7 μg (35 mm Petri dish) or 4.5 μg (100 mm Petri dish) of siRNA targeting the 3′UTR of *DDX6* mRNA (Eurofins Genomics). The sequence of the siRNA targeting the 3′UTR of DDX6 mRNA was: 5′-GGAA CUAUGAAGACUUAAAdTdT-3′.[11] 24 h later, cells were transfected with 1 μg or 5 μg of plasmid DNA (35 mm or 100 mm Petri dish, respectively) via Genjet plus DNA (SignaGen Laboratories). The p.Arg373Gln, p.Cys390Arg, p.Thr391Ile, and p.Thr391Pro

variants were introduced in the previously described FLAG-DDX6-HA plasmid[10] with the InFusion Advantage PCR cloning kit (Clontech) and the following oligonucleotides (Eurofins Genomics):

Arg373Gln_F: 5′-GGAACATCAAAATCGTGTATTTCATGATTTCCGAAATGGCTTATG-3′

Arg373Gln_R: 5′-CGATTTTGATGTTCCTGCCTCATTTTAGCATGAATATAGAAGCAA-3′

Cys390Arg_F: 5′-ATCTTGTTCGCACTGATCTGTTTACCCGAGGTATTGATATACAAG-3′ Cys390Arg_R: 5′-CAGTGCGAACAAGATTGCGGCATAAGCCATTTCGGAAATCATGAA-3′

Thr391Ile_F: 5′-TGTTTGCATTGATCTGTTTACCCGAGGTATTGATATACAAGCTGT-3′

Thr391Ile_R: 5′-AGATCAATGCAAACAAGATTGCGGCATAAGCCATTTCGGAAATCA-3′

Thr391Pro_F: 5′-TTGTTTGCCCTGATCTGTTTACCCGAGGTATTGATATACAAGCTG-3′

Thr391Pro_R: 5′-GATCAGGGCAAACAAGATTGCGGCATAAGCCATTTCGGAAATCAT-3′. Cells were harvested 60 h after plating.

Immunofluorescence

Cells were grown on glass coverslips in 35 mm Petri dish and fixed in methanol for 3 min at −20°C. Cells were blocked 10 min in 2% BSA (bovine serum albumin) in PBS (phosphate-buffered saline), incubated 1 h with the primary antibody, rinsed with PBS, incubated 1 h with a fluorochrome-conjugated secondary antibody, and rinsed in PBS. Slides were mounted in Citifluor (Citifluor). For complementation assays, microscopy was performed on a Leica DMR microscope (Leica) with a 63 × 1.32 oil immersion objective lens. Photographs were taken with a Micromax CCD camera13 (Princeton Instruments) driven by the Metamorph software. For fibroblast imaging, epifluorescence microscopy was performed on an inverted Zeiss Z1 microscope (Zeiss) equipped with a motorized stage using a 63 × 1.4 oil immersion objective lens and running under the Zen software. Photographs were obtained with an Axiocam 506 mono camera (Zeiss). Images were processed with ImageJ. To quantitate PBs, we used the plugin Spot Detector of the open bioimage informatics platform Icy[39] (see Web Resources). Primary antibodies were rabbit DDX6 (Novus Biologicals), rabbit LSM14A (Merck-Millipore), mouse EDC4 (Santa Cruz Biotechnology), and rabbit HA and mouse FLAG M2 (Sigma-Aldrich). Secondary antibodies were purchased from Jackson ImmunoResearch Laboratories.

Immunoprecipitation and Immunoblot Analyses

For immunoprecipitation, HEK293 cells transfected with FLAG-DDX6-HA plasmids were grown in 100 mm Petri dish, washed twice in PBS, scrapped in 2 mL PBS, and pelleted at 360 g. Pellets were resuspended in 0.5 mL lysis buffer (50 mM Tris [pH 7.5], 125 mM NaCl, 0.5% NP40, 1mM EDTA, 1mM EGTA, 1mM DTT, and 5% glycerol) supplemented with RNaseA (10 μg/mL) and 2× EDTA-free protease inhibitor cocktail (Roche Diagnostics). After 30 min of incubation at 4°C, nuclei were pelleted at 500 g for 10 min at 4°C, and proteins from the supernatant were immunoprecipitated according to the following method: 1–3 mg of the cytoplasmic extracts was incubated at 4°C for 2 h with anti-FLAG M2 magnetic beads (Sigma-Aldrich). After washing, bound proteins were eluted with SDS loading buffer. Immunoprecipitated proteins were migrated along with 30 μg of control cytoplasmic lysate and analyzed by immunoblot as described below. Signals were quantified from scanned X-ray films with ImageJ, normalized to the signal obtained with FLAG M2 antibody in the same experiment, and expressed as a relative percentage of binding proteins via the wild-type FLAG-tagged DDX6.

For immunoblot analyses, cytoplasmic extracts were prepared as described,[40] except that soluble and insoluble proteins were separated by centrifugation at 500 g for 10 min at 4°C. After immunoprecipitation, proteins were separated on a NuPage 4%–12% gel (Invitrogen, Thermo Fischer Scientific) and transferred to a PVDF (poly-vinylidene fluoride) membrane (Perkin Elmer). After blocking in PBS containing 5% (wt/vol) nonfat dry milk for 1 h at room temperature, the membrane was incubated with the primary antibody overnight at 4°C, rinsed in PBS, and incubated with horseradish peroxidase-conjugated secondary antibody for 1 h at room temperature. After washing in PBS, proteins were detected with Western lightning plus ECL kit (Perkin Elmer) and visualized by exposure to CL-XPosure film (Pierce, Thermo Fischer Scientific). Primary antibodies included rabbit DDX6 (Novus Biologicals), rabbit ribosomal S6 (Cell Signaling Technology), mouse FLAG M2 (Sigma-Aldrich), rabbit 4E-T (Abcam), rabbit LSM14A (Merck-Millipore), rabbit LSM14B (Sigma-Aldrich), rabbit PAT1B (Cell Signaling Technology), rabbit EDC3 (Abcam), and mouse EDC4 (Santa Cruz Biotechnology). The secondary antibodies were purchased from Jackson ImmunoResearch Laboratories.

Results

Identification of Rare *De Novo* Missense Variants in *DDX6* in Individuals with ID

Individual analyses of the five families did not reveal any known pathogenic variants in genes with associated syndrome(s) closely overlapping the clinical features of the probands. The WES study for Subject 1 (S1) did reveal a *de novo* missense variant in a gene, *DDX6* (GenBank: NM_004397.5; p.Arg373Gln, not previously associated with human disease (Table 1). Data also showed compound-heterozygous missense variants of unknown significance (VUSs) in *DNAH11* (MIM: 603339) (Table S1). *DNAH11* is associated with autosomal-recessive ciliary dyskinesia, primary, 7, with or without *situs inversus* (CILD7) (MIM: 611884), predominately through LoF mutations. The clinical features of CILD7 do not include ID or resemble S1's phenotype. Furthermore, *DNAH11* possesses significantly more missense variation than expected in gnomAD (Z score = −5.61), and ClinVar contains no confirmed pathogenic missense variants. Thus, the VUS was excluded as a candidate. Subject 2 (S2) first underwent an ID gene panel sequencing, singleton WES, and finally WGS of the nuclear family. Among the 146 putative *de novo* variants identified in the proband, only one occurred in a coding region; this variation was a missense change of p.Cys390Arg in *DDX6*. No other candidate variant(s) were identified in coding or genomic regions of genes known to be involved in ID. Two additional *de novo* missense variants in *DDX6*, p.Thr391Ile (in subject 3 [S3]) and p.Thr391Pro (in subject 4 [S4]), were identified by trio WES in unrelated individuals with developmental disorders (GeneDx). Subject 4 carries an additional hemizygous missense VUS in the gene *SLC16A2* (MIM: 30095), associated with Allan-Herndon-Dudley syndrome

Table 1. Pathogenic *DDX6* Variants in Individuals with ID

Coordinate (Hg19/GRCh37)	Variant (GenBank: NM_004397.5)	Exon	Inheritance	Present in gnomAD Database?	CADD	GERP++ RS Score (Vertebrates)	Envision Score	PolyPhen (HumVar)	SIFT	*DDX6* O-E/pLI (gnomAD)	*DDX6* Missense Z Score (gnomAD)	ACMG Classification	Individuals
Chr11: 118627025:C:T	c.1118G>A (p.Arg373Gln)	11	*de novo*	no	31	19.02	0.51 (3%-ile)	1.0 (probably damaging)	0.0 (deleterious)	0.04/1.0	3.93	likely pathogenic (PS2, PM2, PP3)	**S1**
Chr11: 118626975:A:G	c.1168T>C (p.Cys390Arg)	11	*de novo*	no	32	19.02	0.42 (<1%-ile)	1.0 (probably damaging)	0.0 (deleterious)			likely pathogenic (PS2, PM2, PP3)	**S2**
Chr11: 118626971:G:A	c.1172C>T (p.Thr391Ile)	11	*de novo*	no	34	19.02	0.65 (21%-ile)	0.973 (probably damaging)	0.01 (deleterious)			likely pathogenic (PS2, PM2, PP3)	**S3**
Chr11: 118626972:T:G	c.1171A>C (p.Thr391Pro)	11	*de novo*	no	27.6	19.02	0.68 (26%-ile)	0.963 (probably damaging)	0.02 (deleterious)			likely pathogenic (PS2, PM2, PP3)	**S4**
Chr11: 118627028:T:C	c.1115A>G (p.His372Arg)	11	*de novo*	no	25.6	17.86	0.90 (71%-ile)	0.376 (benign)	0.03 (deleterious)			likely pathogenic (PS2, PM2)	**S5**

Envision: 0% (most damaging) – 100% (most like wild type).

(AHDS, MIM: 300523), but this diagnosis does not fit with his clinical history (Table S1). A key feature of males with AHDS is abnormal triiodothyronine (T3) and thyroxine (T4) levels. Repeat thyroid studies including dosages of T3 and T4 (free, total, and reverse) in S4 were all normal. During the final stages of this study, a fifth individual (subject 5 [S5]) with a single *de novo* missense variant of p.His372Arg in *DDX6* was identified by WES. For all individuals, no other variants except the *DDX6* missense changes described above were classified pathogenic or likely to be pathogenic according to ACMG guidelines.

Clinical Features of Individuals Carrying *De Novo* Missense Variants in *DDX6* Exon 11

We could retrieve clinical information for four of the individuals carrying *de novo* missense variants in *DDX6*. These probands are from unrelated families in both the USA and Europe. The affected individuals present with NDD of unknown etiology and range between the ages of 4 to 13 years at last clinical assessment. The parents are noted to be without any significant health problems. Phenotyping of the four affected probands showed overlap of clinical features and minor variation in severity across individuals (Table 2). Clinical features include ID (4/4); DD (4/4); mild to moderate cardiac anomalies (3/4); hypotonia (3/4); gait instability (3/4); and hand, foot, and genitourinary abnormalities (3/4). Other features present include mild to moderate MRI anomalies, a small head circumference (< −2 standard deviations [SDs]), congenital hydronephrosis with vesicoureteral reflux, mild obesity, and autistic traits. The probands also share common facial dysmorphic features including a high forehead, a bulbous nasal tip, widely spaced eyes, arched eyebrows, and low-set ears (Figure 1). Expanded summaries can be found in Supplemental Data: Individual Reports.

DDX6 Missense Variants Found in Affected Individuals Are Absent from Population Databases, Evolutionarily Conserved, and Spatially Clustered within Protein

All *de novo* missense variants identified in affected individuals are located in exon 11 of *DDX6*. This exon is present in all DDX6 isoforms and codes for the conserved motifs QxxR and V within the second RecA-2 domain of the helicase core. The variants have not been observed in the gnomAD database, which contains genetic data from ~140 thousand individuals and is depleted of severe pediatric disorders. *DDX6* is highly intolerant to LoF variants as indicated by gnomAD's (v2.1.1) observed/expected LoF ratio of 0.04 (confident interval [0.01–0.17]), and there is only one heterozygous LoF change reported in the penultimate exon of its canonical isoform (GenBank: NM_004397.5). *DDX6* was also found to have significant intolerance to missense change, indicated by a gnomAD *Z* score of 3.93 (observed/expected ratio of 0.34 [0.29–0.41]), suggesting selection pressure against amino acid changes.[26] In particular, exon 11 (aa 371–391) was

Table 2. Clinical Features of Individuals with *De Novo* Pathogenic Variants in *DDX6*

	Subject 1	Subject 2	Subject 4	Subject 5
Sex/age at last exam	female/5 years	male/6 years	male/10 years	female/13 years
DDX6 variant (GenBank: NM_004397.5)	c.1118G>A (p.Arg373Gln)	c.1168T>C (p.Cys390Arg)	c.1171A>C (p.Thr391Pro)	c.1115A>G (p.His372Arg)
Inheritance	*de novo*	*de novo*	*de novo*	*de novo*
Intellectual disability	+	+	+	+
Developmental delay	+	+	+	+
Speech delay	+ (nonverbal)	+	+	+
Small head circumference (<2 SD)	+	+	–	–
MRI brain anomalies	hypoplastic posterior corpus callosum (27 months)	–	–	wide liquor spaces, thin corpus callosum, mild delay of myelination
Seizures	–	–	history of staring spells, normal EEG	–
Hypotonia	mild, axial	+	–	+
Gait	walked with support until 27 months, many falls from balance issues	–	instability, delayed coordination, toe-walking	trouble with walking, using wheelchair for longer distances
Extremities (hands, feet)	overriding second toes bilaterally	syndactyly II-III of the feet	tapered fingers, hypermobile flat feet	tapered fingers, overriding toes
Facial dysmorphia	hypertelorism, small palpebral fissures, bilateral epicanthus, arched eyebrows	hypertelorism, small palpebral fissures, bilateral epicanthus	arched eyebrows	high-bossing forehead, bitemporal narrowness, telecanthus, epicanthus
Eyes	strabismus, hypermetropia	strabismus, hypermetropia	slight anisocoria	strabismus, hypermetropia
Ears	low-set, petite, and rotated. overfolded superior pinna	low-set	–	overfolded upper helix
Mouth	high, arched palate; smooth prominent philtrum	–	–	–
Heart abnormalities	patent foramen ovale, aberrant right subclavian artery, cardiac murmur	atrial septal defect with spontaneous closing	*no imaging*	patent foramen ovale
Congenital hydronephrosis/ vesicoureteral reflux	+	–	–	–
Feeding or Gastrointestinal difficulties	+ (G-tube)	+	history of abdominal pain, constipation, unexplained elevated LFTs- resolved	–
Genitourinary anomalies	anteriorly placed anus, normal genitalia	cryptorchidism	micropenis	–
Other	recurrent infections, oligohydramnios, malrotated right pelvic kidney	supernumerary nipple, inguinal hernia	hyposmia/anosmia, femoral retroversion, external tibial torsion, progressive striae on legs, photosensitivity with severe eczematous rash on hands, advanced bone age, mild truncal obesity, anxiety, motor stereotypies	single umbilical artery, delayed closure of fontanel, mild hip dysplasia, pes plano valgus, mild obesity, scoliosis

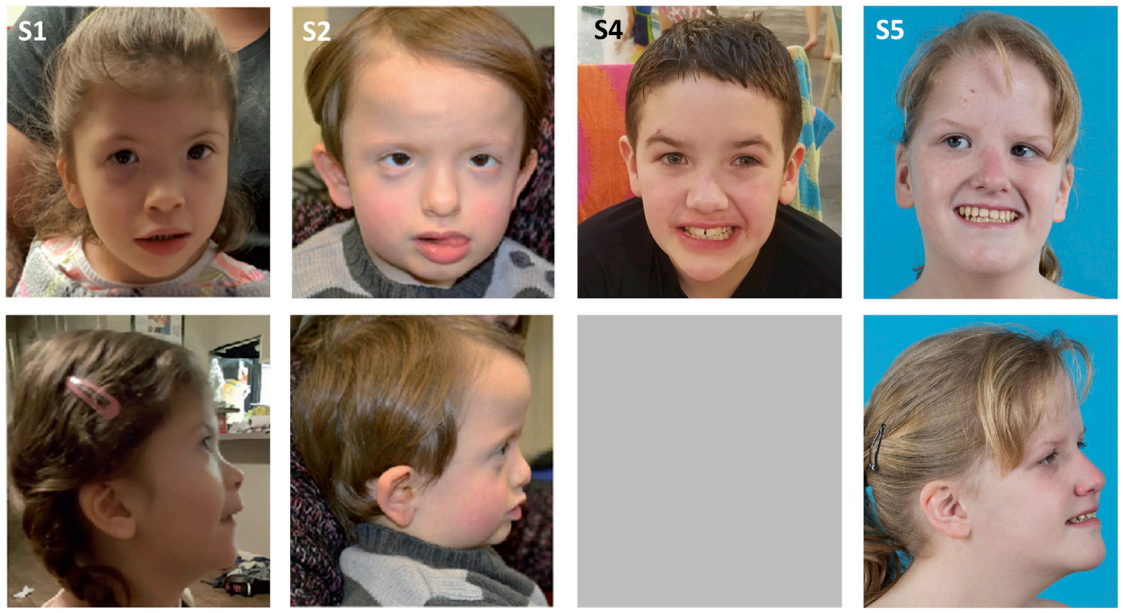

Figure 1. Individuals with Intellectual Disability and Developmental Delay and Rare *De Novo* Missense Variants in *DDX6*
Pictures of individuals with rare *de novo* missense variants in *DDX6* (Subjects S1, S2, S4, and S5).

found highly depleted of nonsynonymous variations in gnomAD (Figure 2A). The specific variants identified in the probands lead to changes at conserved positions and are predicted to be deleterious by *in silico* analysis tools (Table 1 and Figure 2B). The QxxR motif containing Arg373 is conserved in 33/35 DEAD-box family members, and the varying residues are structurally and chemically similar (Glutamine). In Motiv V, residue 390 maintains small, uncharged residues throughout the DEAD-box protein family (35/35), and Thr391 is conserved in every member (Figures S1 and S2). Furthermore, mapping of the variants on a 3D structure of DDX6 in complex with the CNOT1 MIF4G and 4E-T CHD domains[37] showed that proband variants spatially cluster near to or at the protein surface in a region depleted of missense variants in gnomAD populations (Figures 2C and 2D) and close to the 4E-T interaction surface, suggesting that this region is of functional importance for DDX6.

Mutant DDX6 Proteins Are Defective in PB Assembly

Because DDX6 is known to be involved in the formation of cytoplasmic PBs, we first analyzed the presence of PBs in fibroblasts obtained from S2, who carried the p.Cys390Arg change, and from an unrelated age-matched control subject. The cells were analyzed by immunofluorescence that used antibodies against DDX6 and a second PB marker, EDC4 (Figure 3A). Although most fibroblasts from the control subject showed numerous PBs detected by both DDX6 and EDC4 antibodies, only some of the fibroblasts obtained from S2 contained PBs. However, immunoblot analyses indicated that a similar amount of DDX6 protein was present in these cells (Figure S3A), suggesting a functional defect in this variant. Fibroblasts were also obtained from S1, who carried the p.Arg373Gln variant, and from her parents. Again, immunoblot analysis showed similar levels of DDX6 protein in the three cell samples (Figure S3A), whereas immunostaining indicated that the proband's cells contained fewer PBs than the mother's (Figures S3B and S3C). The father's cells grew slowly, however, and possibly related to that, had an intermediate number of PBs: lower than the mother's, but higher than S1's cells (Figures S3B and S3C). To confirm the specific defect of PBs in S1, we therefore submitted the three cell cultures to a mild cold shock at 30°C for 2 h because we showed previously that such a treatment results in increased number and size of PBs in established cell lines.[10] With this treatment, 90% of the parents' cells contained numerous PBs, whereas 70% of S1's cells remained devoid of PBs (Figures 3B and 3C). Moreover, in the 30% of cells with PBs, the numbers remained low, thus confirming a specific PB defect in the proband cells.

We then investigated the ability of the different variant-containing DDX6 proteins to assemble PBs in a model human cell line.[11] Plasmids encoding the four DDX6 initially-identified variants (p.Arg373Gln, p.Cys390Arg, p.Thr391Ile, and p.Thr391Pro) fused to FLAG and HA tags were transfected in HeLa cells (Figure S4A). The variant proteins localized in PBs, as was assessed by immunofluorescence that used LSM14A as a P-body marker (Figure S4B). However, they dramatically affect PB assembly, as was tested by the following complementation assay (Figure 4A). In brief, we depleted cells of endogenous DDX6 by using siRNA targeting the 3′UTR of *DDX6* mRNA (Figure 4B), which resulted, as expected,[11] in PB disassembly (Figures 4A and 4C). 24 h later, cells were transfected with wild-type or mutant FLAG-DDX6-HA plasmids and analyzed 40 h later for

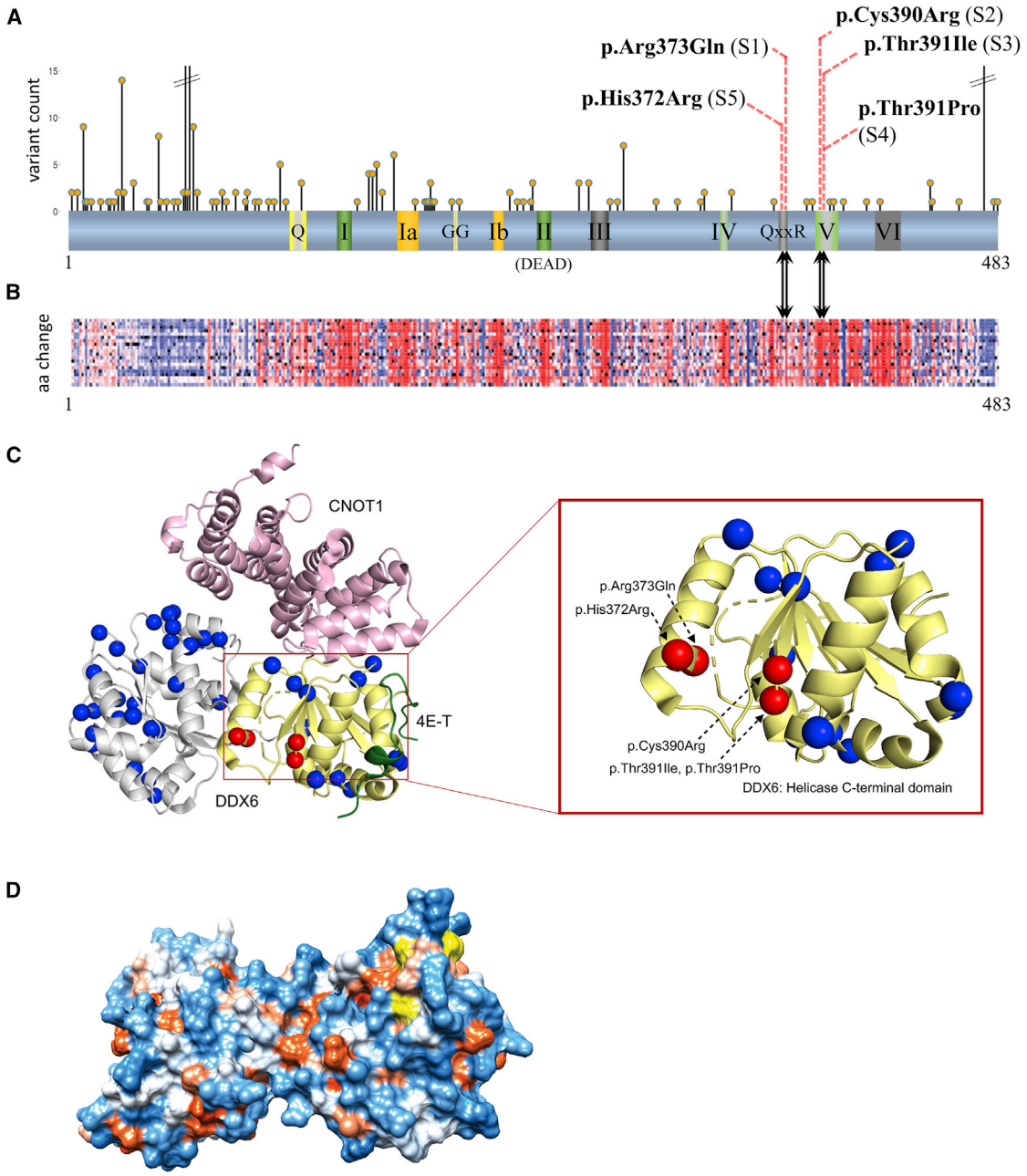

Figure 2. Localization of the Different *De Novo* Missense Variants in *DDX6*

(A) Linear representation of the DDX6 protein (GenBank: NP_004388) with highlighted functional DExD/H-box motifs. *De novo* missense variants identified in individuals with ID are indicated by red dashed lines, and missense variants observed in the gnomAD population are plotted in orange with an indication of the number of individuals carrying them. Motif residue numbers and colors are as follows: motifs Q (115–123) and GG (201–203) in yellow, motifs I (140–146) and II (DEAD) (246–249) in dark green, motifs Ia (171–181) and Ib (222–225) in orange, motif IV (338–340) and V (395–399) in light green, and motifs III (277–279), QxxR (370–373), and VI (419–427) in gray. Motifs Q, I, II, V, and VI are involved in ATP binding, and motifs GG, QxxR, Ia, Ib, IV, and V are involved in RNA binding. Motif III is involved in intramolecular interactions.[13]

(B) A heatmap spanning the linear DDX6 protein representing *in silico* impact (effect) predictions of all possible amino acid substitution mutations in DDX6 from the SNAP2 classifier. Dark red indicates a strong signal for effect, white indicates a weak signal, and blue indicates a strong signal for neutral or no effect.

(C) Mapping of missense variants identified in the gnomAD population (blue spheres) and in probands (red spheres) on a 3D representative structure of DDX6 in complex with the CNOT1 MIF4G (pink) domain and the 4E-T CHD (green) domain (PDB: 5ANR). The two RecA-like units of DDX6 are colored in gray (helicase ATP-binding domain) and yellow (helicase C-terminal domain).

(D) A hydrophobicity surface model of DDX6 (PDB: 4CT5) created with Chimera. Kyte-Doolittle scale coloring was used; colors range from dodger blue for the most hydrophilic, to white at neutral, to orange-red for the most hydrophobic regions. Missense variants identified in probands have been highlighted in yellow.

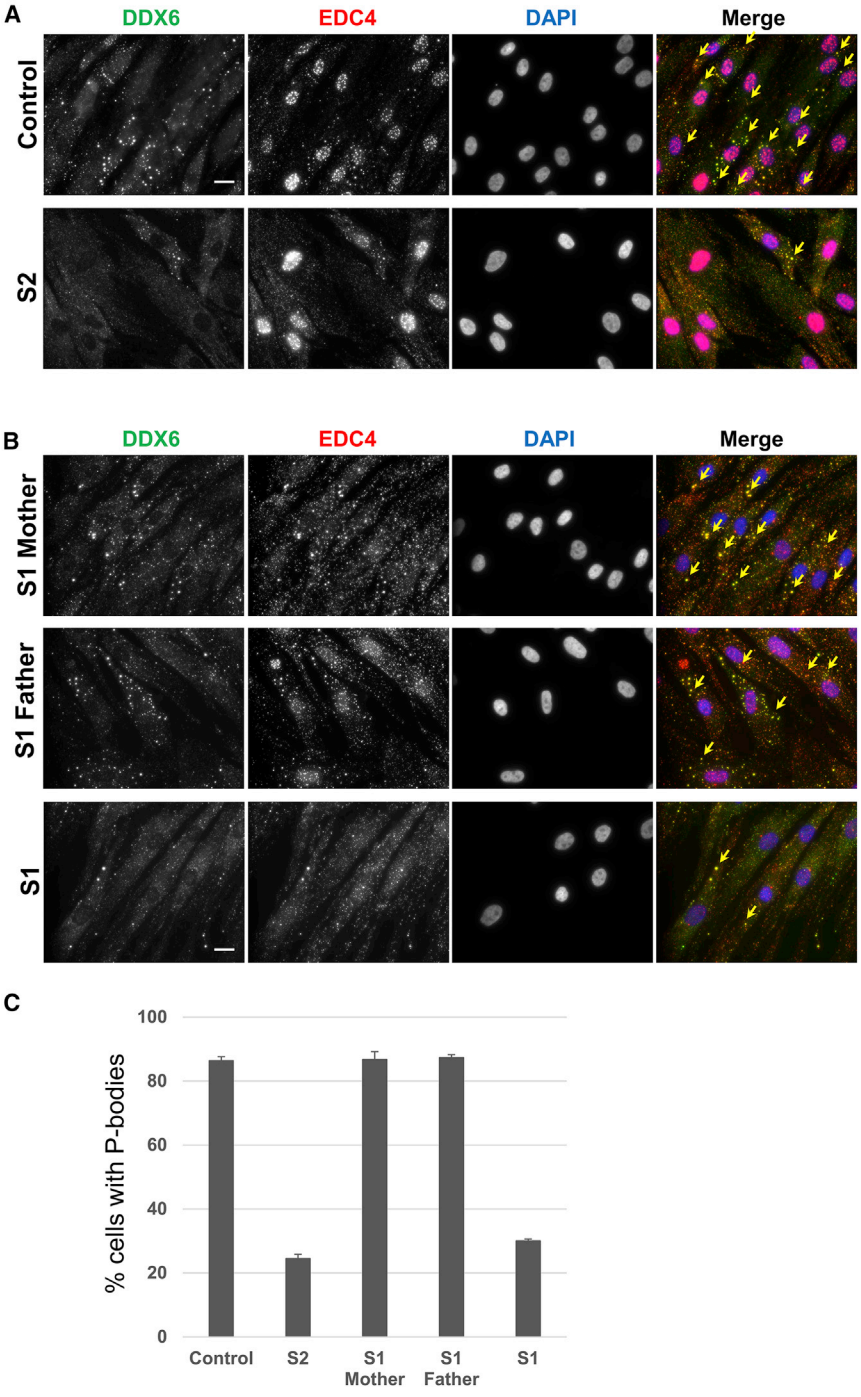

Figure 3. Fibroblasts from Individuals S1 and S2 Contain a Low Number of PBs

(A) Fibroblasts from an unrelated, age-matched control individual and from S2, who carried the DDX6-p.Cys390Arg variant, were immunostained with DDX6 and EDC4 antibodies. Nuclei were stained with DAPI. Arrows point to some selected PBs within cells. The scale bar represents 20 μm.

(B) Fibroblasts from S1, who carried the DDX6-p.Arg373Gln variant, and her healthy parents were analyzed as in (A) except that cells were grown for 2 h at 30°C before fixation. The scale bar represents 20 μm.

(C) Quantification of the fibroblasts with PBs. PB-containing cells were counted and plotted as a percentage of total cells (98 to 126 cells from three and four independent experiments for S2 and S1, respectively). Error bars, SD; t test: $p < 0.0001$ for both probands, as compared with their respective control.

the presence of PBs (Figures 4A and 4C). Whereas the wild-type DDX6 restored PB assembly, no or very few PBs were observed when we used the mutant proteins; there was less than 5% efficiency for the p.Arg373Gln, p.Cys390Arg, and p.The391Ile variants as compared to the wild-type protein, and 17% for the p.Thr391Pro variant (Figures 4A and 4C). We obtained similar results by using EDC4 as a PB marker (Figure S4C). This indicated that the mutant DDX6 proteins were unable to replace the endogenous DDX6 for PB formation.

Mutant DDX6 Proteins Are Defective in Interactions with Protein Partners Key to PB Assembly

Previously, we showed that three factors, DDX6, LSM14A, and 4E-T, are required and their interactions essential for PB assembly.[10,11,41] Mutating the DDX6 FDF-binding pocket (Mut1: four substitutions introduced between residues 320 and 331[9,42,43]) prevents the binding of LSM14A and 4E-T and strongly reduces PB formation.[10] Because the variants identified in *DDX6* are located close to the Mut1 mutations, we hypothesized that they could also alter interactions between DDX6 and these protein partners. To address this question, plasmids encoding wild-type and mutant DDX6 (p.Arg373Gln and p.Cys390Arg) fused to FLAG and HA were transfected in HEK293 cells after depletion of the endogenous DDX6 protein, then immunoprecipitated 48 h later with FLAG antibodies, and the protein complexes were analyzed by immunoblot (Figure 4D). First, both mutant DDX6 proteins showed reduced binding to 4E-T and LSM14A, as compared to wild-type DDX6, and the defect was stronger for the p.Arg373Gln mutant than for the p.Cys390Arg mutant. This is consistent with the inability of these mutants to assemble PBs in the complementation assay. A binding defect was also observed for other DDX6 partners: LSM14B binding was as affected as LSM14A binding in the case of both mutants, whereas other bindings

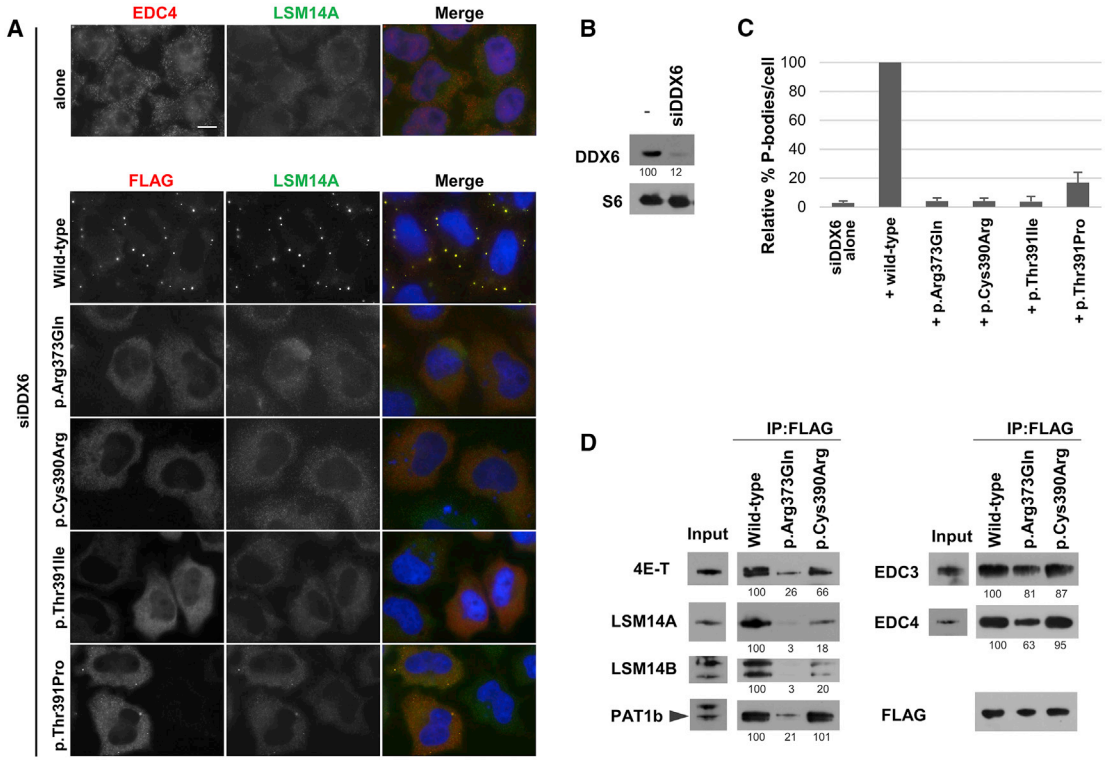

Figure 4. Rare Missense Variants in DDX6 Affect its Interaction with Protein Partners and PB Formation
(A–C) Mutated DDX6 proteins are defective for PB assembly.
(A) Complementation assays. HeLa cells were depleted for endogenous *DDX6* by transfection of a siRNA targeting the *DDX6* 3′UTR at the time of plating (control). After 24 h, cells were transfected or not with indicated FLAG-DDX6-HA plasmids. 40 h later, cells were analyzed by immunofluorescence using the indicated antibodies. The scale bar represents 10 μm.
(B) Protein extracts from cells transfected or not with siRNA were analyzed by immunoblot with the indicated antibodies to verify the DDX6 depletion. The DDX6 signal, normalized using the ribosomal protein S6, is indicated below.
(C) The number of PBs per cell was counted in three independent experiments (21–67 cells per experiment) and expressed as the relative percentage of PBs compared to the complementation with wild-type DDX6. FLAG-DDX6-p.Arg373Gln, -p.Cys390Arg, -p.Thr391Ile, and -p.Thr391Pro correspond to the DDX6 variants identified in subjects 1, 2, 3, and 4, respectively. Error bars, SD; t test: $p < 0.0001$ for all mutants, as compared to wild type.
(D) DDX6 pathogenic variants impair ligand binding. HEK293 cells were depleted for endogenous DDX6 and transfected 24 h later with the indicated FLAG-DDX6-HA plasmids as in (A–C). 48 h later, proteins were extracted in the presence of RNaseA and immunoprecipitated with anti-FLAG M2 antibodies. 10% of the eluates were analyzed by immunoblot using the same antibody (bottom frame), whereas bound proteins were revealed from the remaining eluates by immunoblotting with the indicated antibodies (upper frame). The input corresponds to 30 μg of HEK293 proteins. Indicated under the panels are the percentages of binding proteins compared to immunoprecipitation with the wild-type DDX6, after normalization using the amount of each immunoprecipitated FLAG protein. Similar results were obtained in three to six independent immunoprecipitation experiments.

were defective only in the case of the p.Arg373Gln mutant. This included a strong defect in PAT1B binding and some impairment of EDC3 and EDC4 binding, as well. Overall, the p.Arg373Gln mutant protein was the most defective at interacting with its partners, especially those acting as translation repressors (LSM14A, 4E-T, and PAT1B).

p.Cys390Arg Variant Cells Accumulate mRNAs Involved in Translational Regulation, DDX6 mRNA Targets, and PB-Excluded mRNAs

Transcriptomic (RNAseq) analysis was performed from skin fibroblasts obtained from S2 (who carried the p.Cys390Arg variant) and compared to eight unrelated individuals with other neurodevelopmental or sensorineural conditions unrelated to *DDX6* mutation. More than 1,000 genes were found to be significantly (p-adjusted < 0.05) differentially expressed (DE) (Figure 5A); these included 493 upregulated and 979 downregulated protein-coding genes (Table S2). Enrichment analysis via DAVID[44] demonstrated that the set of genes significantly upregulated was enriched for Gene Ontology "biological process" and "molecular function" terms related to protein translation; these terms included "SRP-dependent cotranslational membrane targeting" (GO: 0006614, fold enrichment FE = 12.5, adjusted p value = 2.0×10^{-18}) or "formation of translation preinitiation complex" (GO: 0001731, FE = 11.3, adjusted p value = 3.3×10^{-2}), or "structural component of the ribosome" (GO: 003735, FE = 5.4, adjusted p value = 1.5×10^{-9}) (Figure 5B). This enrichment was confirmed by analyzing KEGG pathways ("ribosome," map03010 FE = 7.9, adjusted p value = 7.2×10^{-15}). More specifically, 4 out of the 14 expressed eIF3 translation

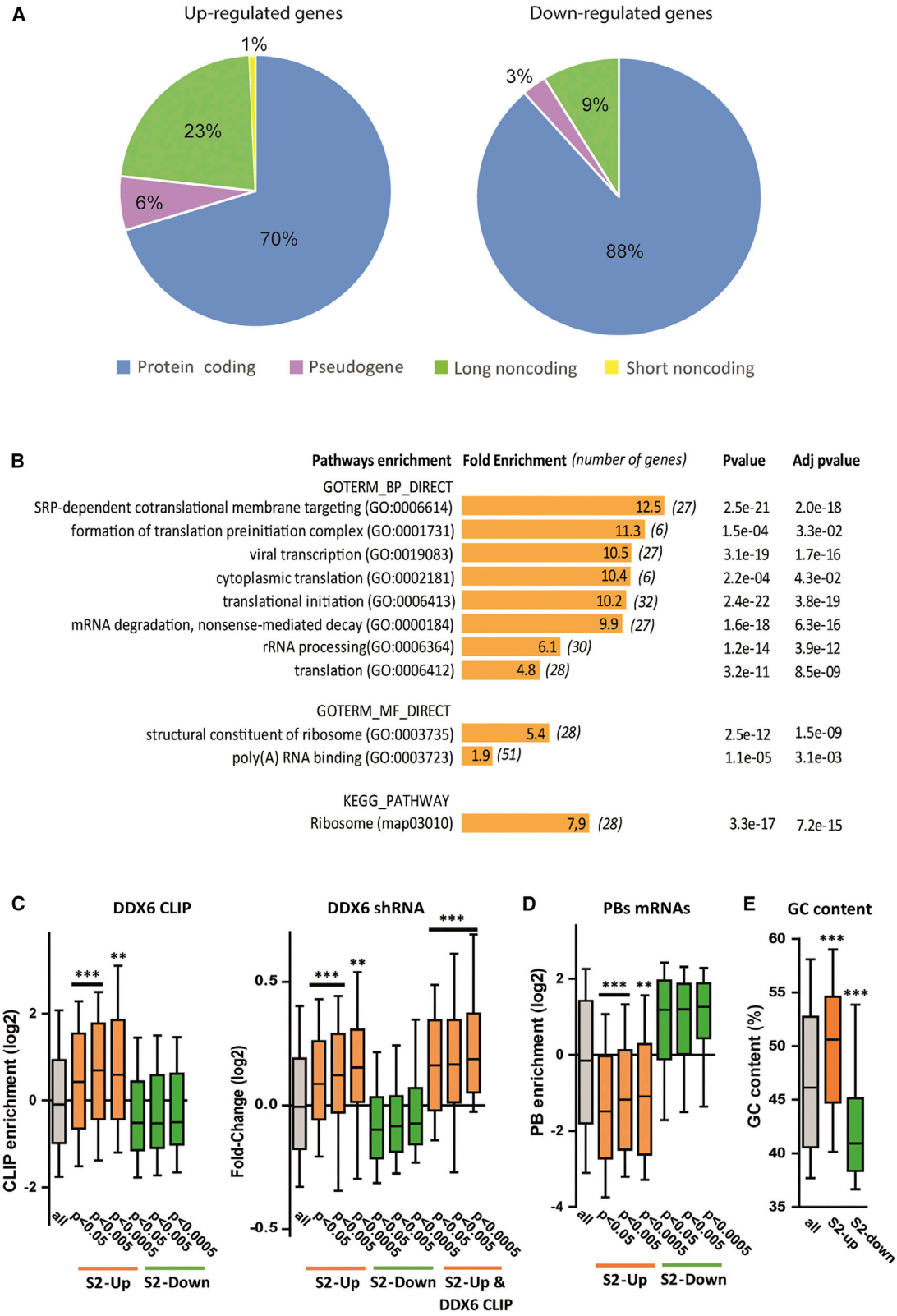

Figure 5. DDX6 Targets and mRNA-Encoding Proteins Involved in Translation Initiation Are Enriched Among Genes Upregulated in Individual S2

(A) A biotype distribution (according to Ensembl) of the differentially-expressed (DE) genes identified in S2.

(B) Pathway enrichment analysis revealed a significant enrichment of the GO terms "Biological Process" and "Molecular Function" related to protein translation, ribosome and RNA processing; it also revealed enrichment for the KEGG pathway "ribosome" among the upregulated genes.

(legend continued on next page)

initiation factor subunit mRNAs and 28 of the 85 expressed ribosomal protein mRNAs were significantly upregulated in S2, whereas none were significantly depleted (Table S3). A subset of the DE genes (*CNOT3*, *HNRNPH2*, *DDX59*, *RPL10*, etc.) encode RNA binding proteins also known to be involved in ID (Table S4).

To investigate relationships between S2's transcriptomic profile and DDX6 function, we took advantage of two datasets available from the ENCODE project, both from the human erythroid cell line K562: (1) a DDX6 cross-linking followed by immunoprecipitation (CLIP) experiment identifying mRNAs that bind to DDX6 and (2) a transcriptome after induction of a stably-transfected *DDX6* shRNA for 48 h identifying mRNAs differentially expressed after DDX6 silencing. If the DDX6-Cys390Arg variant leads to a defect in its function in mRNA decay, we would expect an accumulation of these DDX6 mRNA targets. Indeed, we first observed that significantly enriched mRNAs in S2 fibroblasts were also enriched in ENCODE's DDX6 CLIP experimental data (Figure 5C, left panel), indicating their direct binding to DDX6. Second, enriched mRNAs in S2 also tended to be enriched in the DDX6-silencing dataset (Figure 5C, right panel). Thus, in spite of the differences between the two cell types under comparison (dermal fibroblasts producing a p.Cys390Arg$^{+/-}$ variant DDX6 versus an immortalized erythroid cell line transiently depleted for DDX6), there was a common signature of enriched mRNAs between the two. Furthermore, the enrichment was even stronger for the mRNA subset that was enriched in both the CLIP experiments and the DDX6 silencing experiment (Figure 5C, right panel), indicating that the mRNAs enriched in S2's cells were probably decayed by a DDX6-dependent mechanism that involved direct DDX6 binding.

We have recently shown that mRNAs regulated by DDX6 at the level of decay are localized out of PBs.[12] Accordingly, comparing S2's transcriptome to the mRNA content of purified PBs showed that mRNAs that are enriched in S2's fibroblasts are excluded from PBs (Figure 5D). In the same study, we showed that the mRNAs that are targeted to PBs, in contrast, are regulated at the level of translation. Although translation regulation is not accessible in our transcriptome analysis, the fact that PBs are drastically reduced in S2 strongly suggests that DDX6-dependent translation repression is also affected in these cells. Finally, the mRNAs accumulating in S2 have a high GC content compared to other human genes, whereas the mRNAs depleted are rather AU-rich (Figure 5E). This is consistent with our recent study showing that DDX6 is preferentially involved in the decay of GC-rich mRNAs. Such a high GC content increases the frequency of optimal codons and is therefore observed in actively translated mRNAs.

Discussion

In this study, we describe five rare *de novo* missense variants, identified in individuals with ID, in the RNA helicase *DDX6*. Clinical, genetic, and functional data demonstrated that these missense variants, inducing deficits in DDX6 functions, cause an autosomal-dominant form of intellectual disability associated with mild dysmorphic features. These deficits affect the ability of DDX6 to assemble PBs—constitutive cytoplasmic RNP granules that act in mRNA storage—resulting in their drastic reduction in primary cells of affected individuals, as well as when modeled in human cell lines. Furthermore, co-immunoprecipitation assays showed the pathogenic variants affect DDX6 interactions with protein partners, such as LSM14A and 4E-T, involved in PB assembly, suggesting a mechanism for PB dysfunction and subsequent deregulation of mRNA storage. Interactions with other DDX6 protein partners (PAT1B, EDC3, and EDC4) were differently impacted, depending on the variants. The surface of DDX6 that interacts with these different proteins was reported to be distinct, though overlapping. Therefore, we did not expect that different variants of DDX6 would alter all interactions to the same extent. Additional defects included DDX6 dysfunction in the control of mRNA stability, as transcriptomic analysis of S2 revealed an enrichment of mRNAs that are regulated by DDX6 at the level of decay,[45] in particular mRNA encoding subunits of the translation initiation factor eIF3 and ribosomal proteins (Figure 5F). Many mRNAs also contain in their 5′ UTR a TOP motif that is responsible for their control by the mTORC1 kinase (25 out of the 94 TOP mRNAs previously reported[46] were enriched in S2 cells). Their deregulation could have consequences on the control of cell proliferation/function inside and outside of the CNS.[46,47] Taken together, these findings highlight crucial roles for *DDX6* and/or PBs in proper neurodevelopment.

The missense changes identified in affected individuals cluster in two pairs of amino acids in conserved motifs of

(C) The mRNAs up- (orange boxes) and downregulated (green boxes) in subject 2 (S2) were analyzed for their enrichment in a DDX6 CLIP experiment (left panel) and their differential expression after DDX6 silencing (right panel), both in K562 cells. The analysis was performed with various p value thresholds for the differential expression in S2, as indicated. The distribution of the whole dataset (all) is given for comparison (gray boxes). The whiskers indicate the 10–90 percentiles. Upregulated mRNAs in S2 are preferential DDX6 targets and preferentially upregulated after DDX6 depletion in an erythroid cell line.
(D) Upregulated mRNAs in S2 tend to be excluded from PBs. The mRNAs up- and downregulated in S2 were analyzed for their enrichment in purified PBs, as in (C).
(E) Upregulated mRNAs in S2 tend to have a high GC content. In panels C–E, two-tail Mann-Whitney tests were performed with respect to all mRNAs: ***$p < 0.0005$ and **$p < 0.005$.

the *DDX6* C-terminal RecA domain: residues 372–373, which comprise the second half of the QxxR motif, and 390–391, which lie in motif V[48] (Figures 2A and S1). The substitutions p.Arg373Gln (S1) and p.His372Arg (S5) cause significant alterations to residue properties and likely local protein structure and function. Electrically-charged surface residues like Arg373 are known to promote proper protein folding through solvent interactions, and reactive histidines are most common in protein active sites. The QxxR motif is also involved in interdomain interactions with motif Ia *in vitro* in the yeast DEAD-box protein Mss116p,[49] which was proposed to help form a continuous RNA binding surface and stabilize bound RNA. The change of Cys390 (S2) to a large, electrically-charged arginine, and the conversions of Thr391 (S3 and S4) from a polar threonine to non-polar, unreactive residues (proline and isoleucine), also suggest destabilizing regional changes to the RecA-2 domain. Our co-immunoprecipitation and complementation assays support these predictions with results showing a dysfunction of the variant DDX6 proteins to bind partners through this region and to assemble PBs, respectively. Because the proband fibroblasts have a strong PB deficiency despite the presence of one wild-type allele, it raises the possibility that the DDX6 variants could have some dominant-negative effect on PB assembly. We have previously characterized a clearly dominant-negative DDX6 variant (motif VI mutant HRIG) in an experiment similar to the one described here (Figure S4B), and we found that its expression completely suppressed PBs in the presence of the endogenous DDX6 protein,[11] which is not the case for the probands' variants. We would therefore favor the hypothesis that the low PB assembly results from haploinsufficiency of the wild-type allele.

DDX6 is not the first gene encoding an RNA helicase involved in monogenic forms of ID or NDD. The involvement of *DHX30* in ID was uncovered in 2017 when several *de novo* missense variants also in the RecA domains were reported in twelve individuals with ID, speech impairment, and gait abnormalities.[50] Pathogenic variants including *de novo* truncating and missense changes in RecA domains have also been recently reported in the *DDX3X* gene,[51] located on the X chromosome, in females with ID, hypotonia, movement disorders, and epilepsy. *DDX3X* now represents one of the genes most frequently mutated in ID; it is involved in ~0.5% of ID cases and ~2% of female cases.[52] Interestingly, after sequence alignment of *DDX6* and *DDX3X*, the Arg373 position found mutated in our cohort corresponds to the Arg480 position recurrently mutated in the *DDX3X* cohort of affected individuals, reinforcing the functional importance of this amino acid and the QxxR motif in DEAD-box proteins. LoF variants in another member of this helicase family, *DDX59*, have also been reported to cause an autosomal-recessive form of ID with features of oral-facial-digital syndrome.[53–55]

Interestingly, the phenotypic traits observed in our *DDX6* cohort align well with the syndromes described in individuals with pathogenic variants in *DDX3X* and *DHX30*.[50–52] These include ID, DD, gait abnormalities, cardiac anomalies, and corpus callosum hypoplasia, as well as dysmorphic facial features (high forehead, a bulbous nasal tip, hypertelorism, and arched eyebrows). Conversely, none of the individuals with *DDX6* variants have reported seizures, a feature present in the *DDX3X* and *DHX30* syndromes. This could be an interesting delineation of the *DDX6* cohort and give specific biological insights into the specificity of each DExD/H-box protein. However, seizures are present in only a subset of the *DDX3X* and *DHX30* cohorts (~16% and 25%, respectively), thus study of more individuals with the *DDX6* syndrome is needed to completely exclude seizures as an absent feature. Our cohort also exhibits a degree of variability in their clinical presentations. Individuals S1 and S5 present with mild abnormalities on brain MRI (corpus callosum hypoplasia) and appear to be slightly more affected than the others. Their amino acid changes (p.His372Arg and p.Arg373Gln) lie in the QxxR motif, suggesting that variants in this motif elicit a slightly more severe phenotype than variants in the motif V region. In support of this, co-immunoprecipitation studies demonstrated more drastic defects of protein binding caused by the p.Arg373Gln variant. Because differences in the proband's genetic backgrounds are also likely to contribute to phenotypic variability, the study of more individuals with pathogenic *DDX6* variation will be required to fully answer this question.

DDX6 is widely expressed throughout tissues, and it has some of the highest expression levels in the cerebellar hemispheres. Its expression is regulated in a time-dependent manner in the mouse neocortex during development,[56] and it has been found to be expressed in both mouse[57] and human neural stem cells (NSCs) (data extracted from previous works[58]). DDX6 is further involved in the CNS; it increases the activity of Let-7a, a microRNA important in neuronal differentiation. DDX6 overexpression in mouse NSCs leads to an increase in neuronal differentiation, whereas loss of *DDX6* function inhibits the formation of new neurons.[57] *DDX3X* was also found to be essential for neuronal differentiation and migration, and its inactivation in mice disturbs cortex development and leads to abnormal distribution of neurons in the cortical plate.[59] It is possible the brain anomalies present in DDX6 individuals S1 and S5 result from impaired processes in NSC specification. Although some evidence supports this idea, the exceedingly heterogeneous nature of corpus callosum anomalies requires further *in vivo* work to validate how these pathogenic variants would alter the proliferation, differentiation, or migration of neuronal precursors and synaptic functioning, as well as to identify which mRNAs are deregulated in this cell type.

We have shown that our *DDX6* variants result in failure to form PBs efficiently, and they lead to a decreased number of these RNP granules in the fibroblasts of affected individuals. Lessel et al. recently showed that *DHX30* missense variants, in addition to altering the ability of DHX30 to bind RNA or to exert its ATPase activity, increase the formation of another significant type of RNP granules, stress granules, and this process is associated with a decrease of global

protein translation.[50] The missense variants identified in *DDX3X* were also shown to affect ATPase helicase activity and lead to protein accumulation into RNP granules not well characterized but harboring some translational activity.[59] RNP granule dysfunction in neurons specifically could relate to their polar, asymmetric nature. Indeed, there are a variety of neuronal RNP granules, mostly described in dendrites. Several types of dendritic granules contain PB components and were initially called P-body-like structures[60] or P-bodies.[61] They are important in regulating local translation at the synapse, a process that is essential for synaptic plasticity.[62] However, further attempts to define these granules with the expression of DDX6 and decapping enzymes suggested that these structures were more diverse in neuronal processes than in other cells.[63] In the neuronal soma, RNP granules may be closer to fibroblast PBs in terms of composition and function, but they have not been well characterized. Repression by miRNAs also plays a major role in the control of signaling pathways regulating several steps of cortical development,[64] therefore we can speculate that the different cytoplasmic foci that play roles in the storage of miRNA targets are important for a proper development of the brain.

The present study has taken effort to demonstrate that rare changes in *DDX6* cause PB and mRNA metabolism dysfunction. These DDX6 dysfunctions were observed not only by overexpressing DDX6 in immortalized cell lines but also directly in affected individual's primary fibroblasts (individuals S1 and S2). The use of these non-neuronal cells might only distantly reflect the actual disease pathogenesis in affected individual's brains and other organs. Further transcriptomic and proteomic studies in neuronal cells derived from primary fibroblasts or *in vivo* animal models will shine more light on the specific mechanisms of DDX6-associated pathogenesis in neurodevelopment.

In conclusion, our findings implicate rare *de novo* missense variants in the second RecA domain of *DDX6* in ID. These variants significantly affect DDX6's ability to assemble PBs, resulting in their drastic reduction in cells, and, in the affected individual whose transcriptomic data we have, the significant alteration of the transcriptome landscape. We suggest that rare variants in *DDX6* be considered for pathogenicity in pediatric cases of ID and that this RNA helicase be added to the growing list of NDD- and ID-associated genes. Lastly, together with the recent involvement of *DDX3X* and *DHX30* in ID and similar NDDs, these results also highlight an emerging class of NDD involving RNA helicases.

Supplemental Data

Supplemental Data can be found online at https://doi.org/10.1016/j.ajhg.2019.07.010.

Acknowledgements

The authors thank the families for their participation in the study. The authors also thank the Foundation Jerome Lejeune and Fondation Maladies Rares for their financial support, as well as the Association Paul and Liba Mandel and the CREGEMES (Centre Régional de Génétique Médicale de Strasbourg). This study was also supported by the grant ANR-10-LABX-0030-INRT, a French State fund managed by the Agence Nationale de la Recherche under the frame program Investissements d'Avenir ANR-10-IDEX-0002-02, the National Research Agency (ANR) grant 14-CE09-0013-01ANR, and the Laboratory of Excellence GENMED (Medical Genomics) grant no. ANR-10-LABX-0013 managed by the ANR part of the Investment for the Future program. The authors also want to thank all the people from IGBMC sequencing platform (Bernard Jost, Christelle Thibaut-Charpentier, Céline Keime, and Damien Plassard) for their technical and bioinformatics support. The authors would like to thank all donors who have contributed and participated in TGen's Center for Rare Childhood Disorders Center.

Declaration of Interests

I.W., K.G.M., and K.M. are employees of GeneDx, Inc.

Received: March 19, 2019
Accepted: July 17, 2019
Published: August 15, 2019

Web Resources

Clinvar, https://www.ncbi.nlm.nih.gov/clinvar/
dbSNP, https://www.ncbi.nlm.nih.gov/projects/SNP/
Decipher, https://decipher.sanger.ac.uk/
ENCODE, https://www.encodeproject.org/
ExAC Browser (Beta) | Exome Aggregation Consortium, http://exac.broadinstitute.org/
GeneDx ClinVar submissions page, https://www.ncbi.nlm.nih.gov/clinvar/submitters/26957/
GeneMatcher, https://genematcher.org/
GnomAD Exome Variant Server, https://gnomad.broadinstitute.org/
Icy, http://icy.bioimageanalysis.org
Integrative Genomics Viewer (IGV), https://www.broadinstitute.org/igv/
Mutation Nomenclature, http://www.hgvs.org/mutnomen/recs.html
OMIM, http://www.omim.org/
UCSC, http://genome.ucsc.edu/
SNAP2, https://rostlab.org/services/snap2web/
SysID Database, https://sysid.cmbi.umcn.nl/
Protein Data Bank (PDB), https://www.pdb.org

References

1. Vissers, L.E.L.M., Gilissen, C., and Veltman, J.A. (2016). Genetic studies in intellectual disability and related disorders. Nat. Rev. Genet. *17*, 9–18.
2. Lelieveld, S.H., Wiel, L., Venselaar, H., Pfundt, R., Vriend, G., Veltman, J.A., Brunner, H.G., Vissers, L.E.L.M., and Gilissen, C. (2017). Spatial clustering of de novo missense mutations identifies candidate neurodevelopmental disorder-associated genes. Am. J. Hum. Genet. *101*, 478–484.
3. Bardoni, B., Abekhoukh, S., Zongaro, S., and Melko, M. (2012). Intellectual disabilities, neuronal posttranscriptional RNA

metabolism, and RNA-binding proteins: Three actors for a complex scenario. Prog. Brain Res. *197*, 29–51.
4. Sartor, F., Anderson, J., McCaig, C., Miedzybrodzka, Z., and Müller, B. (2015). Mutation of genes controlling mRNA metabolism and protein synthesis predisposes to neurodevelopmental disorders. Biochem. Soc. Trans. *43*, 1259–1265.
5. Oberlé, I., Rousseau, F., Heitz, D., Kretz, C., Devys, D., Hanauer, A., Boué, J., Bertheas, M.F., and Mandel, J.L. (1991). Instability of a 550-base pair DNA segment and abnormal methylation in fragile X syndrome. Science *252*, 1097–1102.
6. Hagerman, R.J., Berry-Kravis, E., Hazlett, H.C., Bailey, D.B., Jr., Moine, H., Kooy, R.F., Tassone, F., Gantois, I., Sonenberg, N., Mandel, J.L., and Hagerman, P.J. (2017). Fragile X syndrome. Nat. Rev. Dis. Primers *3*, 17065.
7. Jankowsky, E., and Fairman, M.E. (2007). RNA helicases–one fold for many functions. Curr. Opin. Struct. Biol. *17*, 316–324.
8. Abdelhaleem, M., Maltais, L., and Wain, H. (2003). The human DDX and DHX gene families of putative RNA helicases. Genomics *81*, 618–622.
9. Ozgur, S., Basquin, J., Kamenska, A., Filipowicz, W., Standart, N., and Conti, E. (2015). Structure of a human 4E-T/DDX6/CNOT1 complex reveals the different interplay of DDX6-binding proteins with the CCR4-NOT complex. Cell Rep. *13*, 703–711.
10. Ayache, J., Bénard, M., Ernoult-Lange, M., Minshall, N., Standart, N., Kress, M., and Weil, D. (2015). P-body assembly requires DDX6 repression complexes rather than decay or Ataxin2/2L complexes. Mol. Biol. Cell *26*, 2579–2595.
11. Minshall, N., Kress, M., Weil, D., and Standart, N. (2009). Role of p54 RNA helicase activity and its C-terminal domain in translational repression, P-body localization and assembly. Mol. Biol. Cell *20*, 2464–2472.
12. Hubstenberger, A., Courel, M., Bénard, M., Souquere, S., Ernoult-Lange, M., Chouaib, R., Yi, Z., Morlot, J.-B., Munier, A., Fradet, M., et al. (2017). P-Body purification reveals the condensation of repressed mRNA regulons. Mol. Cell *68*, 144–157.e5.
13. Standart, N., and Weil, D. (2018). P-bodies: Cytosolic droplets for coordinated mRNA storage. Trends Genet. *34*, 612–626.
14. Sobreira, N., Schiettecatte, F., Valle, D., and Hamosh, A. (2015). GeneMatcher: A matching tool for connecting investigators with an interest in the same gene. Hum. Mutat. *36*, 928–930.
15. Li, H., and Durbin, R. (2009). Fast and accurate short read alignment with Burrows-Wheeler transform. Bioinformatics *25*, 1754–1760.
16. McKenna, A., Hanna, M., Banks, E., Sivachenko, A., Cibulskis, K., Kernytsky, A., Garimella, K., Altshuler, D., Gabriel, S., Daly, M., and DePristo, M.A. (2010). The Genome Analysis Toolkit: A MapReduce framework for analyzing next-generation DNA sequencing data. Genome Res. *20*, 1297–1303.
17. Van der Auwera, G.A., Carneiro, M.O., Hartl, C., Poplin, R., Del Angel, G., Levy-Moonshine, A., Jordan, T., Shakir, K., Roazen, D., Thibault, J., et al. (2013). From FastQ data to high confidence variant calls: The Genome Analysis Toolkit best practices pipeline. Curr Protoc Bioinformatics *43*, 11.10.1–33.
18. Cingolani, P., Platts, A., Wang, L., Coon, M., Nguyen, T., Wang, L., Land, S.J., Lu, X., and Ruden, D.M. (2012). A program for annotating and predicting the effects of single nucleotide polymorphisms, SnpEff: SNPs in the genome of Drosophila melanogaster strain w1118; iso-2; iso-3. Fly (Austin) *6*, 80–92.
19. Thevenon, J., Duffourd, Y., Masurel-Paulet, A., Lefebvre, M., Feillet, F., El Chehadeh-Djebbar, S., St-Onge, J., Steinmetz, A., Huet, F., Chouchane, M., et al. (2016). Diagnostic odyssey in severe neurodevelopmental disorders: Toward clinical whole-exome sequencing as a first-line diagnostic test. Clin. Genet. *89*, 700–707.
20. Rimmer, A., Phan, H., Mathieson, I., Iqbal, Z., Twigg, S.R.F., Wilkie, A.O.M., McVean, G., Lunter, G.; and WGS500 Consortium (2014). Integrating mapping-, assembly- and haplotype-based approaches for calling variants in clinical sequencing applications. Nat. Genet. *46*, 912–918.
21. Geoffroy, V., Pizot, C., Redin, C., Piton, A., Vasli, N., Stoetzel, C., Blavier, A., Laporte, J., and Muller, J. (2015). VaRank: A simple and powerful tool for ranking genetic variants. PeerJ *3*, e796.
22. Bartenhagen, C., and Dugas, M. (2016). Robust and exact structural variation detection with paired-end and soft-clipped alignments: SoftSV compared with eight algorithms. Brief. Bioinform. *17*, 51–62.
23. Backenroth, D., Homsy, J., Murillo, L.R., Glessner, J., Lin, E., Brueckner, M., Lifton, R., Goldmuntz, E., Chung, W.K., and Shen, Y. (2014). CANOES: Detecting rare copy number variants from whole exome sequencing data. Nucleic Acids Res. *42*, e97.
24. Geoffroy, V., Herenger, Y., Kress, A., Stoetzel, C., Piton, A., Dollfus, H., and Muller, J. (2018). AnnotSV: An integrated tool for structural variations annotation. Bioinformatics *34*, 3572–3574.
25. Tanaka, A.J., Cho, M.T., Retterer, K., Jones, J.R., Nowak, C., Douglas, J., Jiang, Y.-H., McConkie-Rosell, A., Schaefer, G.B., Kaylor, J., et al. (2016). De novo pathogenic variants in CHAMP1 are associated with global developmental delay, intellectual disability, and dysmorphic facial features. Cold Spring Harb. Mol. Case Stud. *2*, a000661.
26. Lek, M., Karczewski, K.J., Minikel, E.V., Samocha, K.E., Banks, E., Fennell, T., O'Donnell-Luria, A.H., Ware, J.S., Hill, A.J., Cummings, B.B., et al.; Exome Aggregation Consortium (2016). Analysis of protein-coding genetic variation in 60,706 humans. Nature *536*, 285–291.
27. Kircher, M., Witten, D.M., Jain, P., O'Roak, B.J., Cooper, G.M., and Shendure, J. (2014). A general framework for estimating the relative pathogenicity of human genetic variants. Nat. Genet. *46*, 310–315.
28. Cooper, G.M., Stone, E.A., Asimenos, G., Green, E.D., Batzoglou, S., Sidow, A.; and NISC Comparative Sequencing Program (2005). Distribution and intensity of constraint in mammalian genomic sequence. Genome Res. *15*, 901–913.
29. Ng, P.C., and Henikoff, S. (2003). SIFT: Predicting amino acid changes that affect protein function. Nucleic Acids Res. *31*, 3812–3814.
30. Adzhubei, I.A., Schmidt, S., Peshkin, L., Ramensky, V.E., Gerasimova, A., Bork, P., Kondrashov, A.S., and Sunyaev, S.R. (2010). A method and server for predicting damaging missense mutations. Nat. Methods *7*, 248–249.
31. Hecht, M., Bromberg, Y., and Rost, B. (2015). Better prediction of functional effects for sequence variants. BMC Genomics *16* (*Suppl 8*), S1.
32. Gray, V.E., Hause, R.J., Luebeck, J., Shendure, J., and Fowler, D.M. (2018). Quantitative missense variant effect prediction using large-scale mutagenesis data. Cell Syst. *6*, 116–124.e3.
33. Richards, S., Aziz, N., Bale, S., Bick, D., Das, S., Gastier-Foster, J., Grody, W.W., Hegde, M., Lyon, E., Spector, E., et al.; ACMG

Laboratory Quality Assurance Committee (2015). Standards and guidelines for the interpretation of sequence variants: A joint consensus recommendation of the American College of Medical Genetics and Genomics and the Association for Molecular Pathology. Genet. Med. *17*, 405–424.
34. Anders, S., Pyl, P.T., and Huber, W. (2015). HTSeq–a Python framework to work with high-throughput sequencing data. Bioinformatics *31*, 166–169.
35. Anders, S., and Huber, W. (2010). Differential expression analysis for sequence count data. Genome Biol. *11*, R106.
36. Benjamini, Y. (1995). Controlling the false discovery rate: A practical and powerful approach to multiple testing. Journal of the Royal Statistical Society. Series B *57*, 289–300.
37. Mathys, H., Basquin, J., Ozgur, S., Czarnocki-Cieciura, M., Bonneau, F., Aartse, A., Dziembowski, A., Nowotny, M., Conti, E., and Filipowicz, W. (2014). Structural and biochemical insights to the role of the CCR4-NOT complex and DDX6 ATPase in microRNA repression. Mol. Cell *54*, 751–765.
38. Pettersen, E.F., Goddard, T.D., Huang, C.C., Couch, G.S., Greenblatt, D.M., Meng, E.C., and Ferrin, T.E. (2004). UCSF Chimera–a visualization system for exploratory research and analysis. J. Comput. Chem. *25*, 1605–1612.
39. de Chaumont, F., Dallongeville, S., Chenouard, N., Hervé, N., Pop, S., Provoost, T., Meas-Yedid, V., Pankajakshan, P., Lecomte, T., Le Montagner, Y., et al. (2012). Icy: An open bioimage informatics platform for extended reproducible research. Nat. Methods *9*, 690–696.
40. Ernoult-Lange, M., Baconnais, S., Harper, M., Minshall, N., Souquere, S., Boudier, T., Bénard, M., Andrey, P., Pierron, G., Kress, M., et al. (2012). Multiple binding of repressed mRNAs by the P-body protein Rck/p54. RNA *18*, 1702–1715.
41. Kamenska, A., Simpson, C., Vindry, C., Broomhead, H., Bénard, M., Ernoult-Lange, M., Lee, B.P., Harries, L.W., Weil, D., and Standart, N. (2016). The DDX6-4E-T interaction mediates translational repression and P-body assembly. Nucleic Acids Res. *44*, 6318–6334.
42. Tritschler, F., Eulalio, A., Helms, S., Schmidt, S., Coles, M., Weichenrieder, O., Izaurralde, E., and Truffault, V. (2008). Similar modes of interaction enable Trailer Hitch and EDC3 to associate with DCP1 and Me31B in distinct protein complexes. Mol. Cell. Biol. *28*, 6695–6708.
43. Sharif, H., Ozgur, S., Sharma, K., Basquin, C., Urlaub, H., and Conti, E. (2013). Structural analysis of the yeast Dhh1-Pat1 complex reveals how Dhh1 engages Pat1, Edc3 and RNA in mutually exclusive interactions. Nucleic Acids Res. *41*, 8377–8390.
44. Huang, D.W., Sherman, B.T., Tan, Q., Kir, J., Liu, D., Bryant, D., Guo, Y., Stephens, R., Baseler, M.W., Lane, H.C., and Lempicki, R.A. (2007). DAVID Bioinformatics Resources: Expanded annotation database and novel algorithms to better extract biology from large gene lists. Nucleic Acids Res. *35*, W169–W175.
45. Courel, M., Clement, Y., Foretek, D., Vidal, O., Yi, Z., Kress, M., Vindry, C., Benard, M., Bossevain, C., Antoniewski, C., et al. (2018). GC content shapes mRNA decay and storage in human cells. bioRxiv.
46. Thoreen, C.C., Chantranupong, L., Keys, H.R., Wang, T., Gray, N.S., and Sabatini, D.M. (2012). A unifying model for mTORC1-mediated regulation of mRNA translation. Nature *485*, 109–113.
47. Costa-Mattioli, M., and Monteggia, L.M. (2013). mTOR complexes in neurodevelopmental and neuropsychiatric disorders. Nat. Neurosci. *16*, 1537–1543.
48. Sengoku, T., Nureki, O., Nakamura, A., Kobayashi, S., and Yokoyama, S. (2006). Structural basis for RNA unwinding by the DEAD-box protein Drosophila Vasa. Cell *125*, 287–300.
49. Bifano, A.L., Turk, E.M., and Caprara, M.G. (2010). Structure-guided mutational analysis of a yeast DEAD-box protein involved in mitochondrial RNA splicing. J. Mol. Biol. *398*, 429–443.
50. Lessel, D., Schob, C., Küry, S., Reijnders, M.R.F., Harel, T., Eldomery, M.K., Coban-Akdemir, Z., Denecke, J., Edvardson, S., Colin, E., et al.; DDD study; and C4RCD Research Group (2017). De novo missense mutations in DHX30 impair global translation and cause a neurodevelopmental disorder. Am. J. Hum. Genet. *101*, 716–724.
51. Snijders Blok, L., Madsen, E., Juusola, J., Gilissen, C., Baralle, D., Reijnders, M.R.F., Venselaar, H., Helsmoortel, C., Cho, M.T., Hoischen, A., et al.; DDD Study (2015). Mutations in DDX3X are a common cause of unexplained intellectual disability with gender-specific effects on Wnt signaling. Am. J. Hum. Genet. *97*, 343–352.
52. Wang, X., Posey, J.E., Rosenfeld, J.A., Bacino, C.A., Scaglia, F., Immken, L., Harris, J.M., Hickey, S.E., Mosher, T.M., Slavotinek, A., et al.; Undiagnosed Diseases Network (2018). Phenotypic expansion in *DDX3X* - a common cause of intellectual disability in females. Ann. Clin. Transl. Neurol. *5*, 1277–1285.
53. Shamseldin, H.E., Rajab, A., Alhashem, A., Shaheen, R., Al-Shidi, T., Alamro, R., Al Harassi, S., and Alkuraya, F.S. (2013). Mutations in DDX59 implicate RNA helicase in the pathogenesis of orofaciodigital syndrome. Am. J. Hum. Genet. *93*, 555–560.
54. Salpietro, V., Efthymiou, S., Manole, A., Maurya, B., Wiethoff, S., Ashokkumar, B., Cutrupi, M.C., Dipasquale, V., Manti, S., Botia, J.A., et al. (2018). A loss-of-function homozygous mutation in DDX59 implicates a conserved DEAD-box RNA helicase in nervous system development and function. Hum. Mutat. *39*, 187–192.
55. Faily, S., Perveen, R., Urquhart, J., Chandler, K., and Clayton-Smith, J. (2017). Confirmation that mutations in DDX59 cause an autosomal recessive form of oral-facial-digital syndrome: Further delineation of the DDX59 phenotype in two new families. Eur. J. Med. Genet. *60*, 527–532.
56. Telley, L., Govindan, S., Prados, J., Stevant, I., Nef, S., Dermitzakis, E., Dayer, A., and Jabaudon, D. (2016). Sequential transcriptional waves direct the differentiation of newborn neurons in the mouse neocortex. Science *351*, 1443–1446.
57. Nicklas, S., Okawa, S., Hillje, A.-L., González-Cano, L., Del Sol, A., and Schwamborn, J.C. (2015). The RNA helicase DDX6 regulates cell-fate specification in neural stem cells via miRNAs. Nucleic Acids Res. *43*, 2638–2654.
58. Quartier, A., Chatrousse, L., Redin, C., Keime, C., Haumesser, N., Maglott-Roth, A., Brino, L., Le Gras, S., Benchoua, A., Mandel, J.-L., and Piton, A. (2018). Genes and pathways regulated by androgens in human neural cells, potential candidates for the male excess in autism spectrum disorder. Biol. Psychiatry *84*, 239–252.
59. Lennox, A.L., Jiang, R., Suit, L., Fregeau, B., Sheehan, C.J., Aldinger, K.A., Moey, C., Lobach, I., Mirzaa, G., Afenjar, A., et al. (2018). Pathogenic DDX3X mutations impair RNA metabolism and neurogenesis during fetal cortical development. BioRxiv. https://doi.org/10.1101/317974.

60. Cougot, N., Bhattacharyya, S.N., Tapia-Arancibia, L., Bordonné, R., Filipowicz, W., Bertrand, E., and Rage, F. (2008). Dendrites of mammalian neurons contain specialized P-body-like structures that respond to neuronal activation. J. Neurosci. *28*, 13793–13804.
61. Zeitelhofer, M., Karra, D., Macchi, P., Tolino, M., Thomas, S., Schwarz, M., Kiebler, M., and Dahm, R. (2008). Dynamic interaction between P-bodies and transport ribonucleoprotein particles in dendrites of mature hippocampal neurons. J. Neurosci. *28*, 7555–7562.
62. Kiebler, M.A., and Bassell, G.J. (2006). Neuronal RNA granules: Movers and makers. Neuron *51*, 685–690.
63. Miller, L.C., Blandford, V., McAdam, R., Sanchez-Carbente, M.R., Badeaux, F., DesGroseillers, L., and Sossin, W.S. (2009). Combinations of DEAD box proteins distinguish distinct types of RNA: Protein complexes in neurons. Mol. Cell. Neurosci. *40*, 485–495.
64. Lennox, A.L., Mao, H., and Silver, D.L. (2018). RNA on the brain: Emerging layers of post-transcriptional regulation in cerebral cortex development. Wiley Interdiscip. Rev. Dev. Biol. *7*.